

SIGNATURES OF PLANETS AND PROTOPLANETS IN THE GALACTIC CENTER: A CLUE TO UNDERSTAND THE G2 CLOUD?

MICHELA MAPELLI¹ & EMANUELE RIPAMONTI^{2,1}

Draft version June 1, 2021

ABSTRACT

Several hundred young stars lie in the innermost parsec of our Galaxy. The super-massive black hole (SMBH) might capture planets orbiting these stars, and bring them onto nearly radial orbits. The same fate might occur to planetary embryos (PEs), i.e. protoplanets born from gravitational instabilities in protoplanetary disks. In this paper, we investigate the emission properties of rogue planets and PEs in the Galactic center. In particular, we study the effects of photoevaporation, caused by the ultraviolet background. Rogue planets can hardly be detected by current or forthcoming facilities, unless they are tidally disrupted and accrete onto the SMBH. In contrast, photoevaporation of PEs (especially if the PE is being tidally stripped) might lead to a recombination rate as high as $\approx 10^{45} \text{ s}^{-1}$, corresponding to a Brackett- γ luminosity $L_{\text{Br-}\gamma} \approx 10^{31} \text{ erg s}^{-1}$, very similar to the observed luminosity of the dusty object G2. We critically discuss the possibility that G2 is a rogue PE, and the major uncertainties of this model.

Subject headings: Galaxy: center – black hole physics – planets and satellites: gaseous planets

1. INTRODUCTION

The Galactic center (GC) is one of the most studied and yet enigmatic places in our Universe. It is exceptionally crowded: it hosts a supermassive black hole (SMBH, Gillessen et al. 2009a), a dense star cluster of old stars (Schödel et al. 2007), several thousand solar masses of molecular, atomic and ionized gas (Liu et al. 2012; Jackson et al. 1993; Scoville et al. 2003), and a few hundred young stars (Genzel et al. 2003; Paumard et al. 2006; Bartko et al. 2009; Lu et al. 2009, 2013). A relevant fraction ($\sim 20\%$) of the young massive stars lie in the so called clockwise disk (Paumard et al. 2006; Bartko et al. 2009; Lu et al. 2009, 2013), a thin disk with inner radius $\sim 0.04 \text{ pc}$ and outer radius $\sim 0.13 \text{ pc}$ (Yelda et al. 2014). A small group of B-type stars (~ 20 objects, forming the so called S-cluster) orbit around the SMBH with semi-major axes $< 0.04 \text{ pc}$, with isotropically oriented orbital planes, and with high eccentricities (approximately following a thermal distribution, Gillessen et al. 2009b). The formation of the young stars in the clockwise disk and in the S-cluster has been a puzzle for a long time, because the tidal shear from the SMBH disrupts molecular clouds, preventing star formation in normal conditions.

A faint dusty object (named G2, Gillessen et al. 2012) has been observed on a very eccentric orbit around the SMBH, with a periape distance of only $\sim 200 \text{ AU}$ (Witzel et al. 2014; Pfuhl et al. 2014). G2 has transited at periape in Spring 2014, avoiding complete tidal disruption. The nature of G2 is still enigmatic: a pure gas cloud (Gillessen et al. 2012; Schartmann et al. 2012; Burkert et al. 2012; Shcherbakov 2014; De Colle et al. 2014; McCourt et al. 2015), a dust-enshrouded low-

mass star (Scoville & Burkert 2013; Ballone et al. 2013; Witzel et al. 2014), a low-mass star with a protoplanetary disk (Murray-Clay & Loeb 2012), a star disrupted by a stellar-mass black hole (Miralda-Escudé 2012), a star that underwent partial tidal disruption by the SMBH (Guillochon et al. 2014), a merger between two stars (Prodan et al. 2015), and a nova outburst (Meyer & Meyer-Hofmeister 2012) have been proposed to explain its properties (see Mapelli & Gualandris 2015 for a recent review).

Planets have not been detected in the GC so far, but the destiny of planets, asteroids and planetesimals has been investigated by several authors. Collisions of planets or asteroids have been proposed to lead to the formation of a dusty torus around SMBHs (Nayakshin et al. 2012). The tidal disruption of planetesimals by the SMBH has been invoked as mechanism to explain the daily infrared flares of SgrA* (Cadez et al. 2008; Kostić et al. 2009; Zubovas et al. 2012; Hamers & Portegies Zwart 2015). Tidal disruptions of planets are expected to be much less frequent, but more dramatic events, and might account for the possible past activity of SgrA* (Revnivtsev et al. 2004; Terrier et al. 2010; Ponti et al. 2010; Zubovas et al. 2012). A system composed of a low-mass star and its protoplanetary disk is one of the most viable scenarios to explain the G2 object (Murray-Clay & Loeb 2012). Recently, radio-continuum observations revealed 44 partially resolved compact sources in the innermost $\sim 0.1 \text{ pc}$, interpreted as candidate photoevaporative protoplanetary disks (Yusef-Zadeh et al. 2015).

The aim of this paper is to investigate the main possible signatures of planets and planetary embryos (PEs, i.e. dense gas clouds produced by local gravitational instabilities in a protoplanetary disk, Kuiper 1951; Cameron 1978; Boss 1997; Durisen et al. 2007) in the GC. In Sections 2 and 3, we describe the mechanisms that might produce rogue planets and PEs in the GC, and we estimate the mass loss that planets and PEs undergo because

¹ INAF-Osservatorio Astronomico di Padova, Vicolo dell'Osservatorio 5, I-35122, Padova, Italy; michela.mapelli@oapd.inaf.it

² Dipartimento di Fisica e Astronomia Galileo Galilei, University of Padova, Vicolo dell'Osservatorio 3, I-35122, Padova, Italy

of photoevaporation by the ultraviolet (UV) background. In Section 4, we discuss the observational signatures of planets and PEs, with particular attention for the Br γ line emission), and we suggest that the G2 object might be associated with a rogue PE. Section 5 is a summary of our main results.

2. ROGUE PLANETS

2.1. Tidal capture by the SMBH

The tidal shear of the SMBH can unbind a planet from its star if the initial semi-major axis of the planet orbit is

$$a_p \geq 19 \text{ AU} \left(\frac{d}{0.01 \text{ pc}} \right) \left(\frac{m_*}{10 M_\odot} \right)^{1/3} \left(\frac{4 \times 10^6 M_\odot}{M_{\text{BH}}} \right)^{1/3} \quad (1)$$

where d is the periape of the star orbit around the SMBH, m_* is the star mass, and M_{BH} is the SMBH mass. Fig. 1 shows a_p as a function of d , for $m_* = 1$ and $10 M_\odot$.

One of the two members of the split binary (generally the most massive one) receives a kick that makes it more bound to the SMBH, while the other member (generally the less massive one) becomes less bound. The less bound object might be ejected, while the remaining one is captured by the SMBH (e.g. Ginsburg et al. 2012). On the other hand, the typical variation δ_v of the velocity of the planet is (Pfahl 2005)

$$\begin{aligned} \delta_v &\sim \sqrt{2} \left(\frac{G m_*}{a_p} \right)^{1/2} \left(\frac{M_{\text{BH}}}{m_*} \right)^{1/6} \\ &\sim 170 \text{ km s}^{-1} \left(\frac{m_*}{1 M_\odot} \right)^{1/2} \left(\frac{10 \text{ AU}}{a_p} \right)^{1/2} \left(\frac{M_{\text{BH}}/m_*}{4 \times 10^6} \right)^{1/6} \quad (2) \end{aligned}$$

since δ_v is lower than the Keplerian velocity around the SMBH at $d = 0.01 \text{ pc}$ ($\sim 1300 \text{ km s}^{-1}$), it is plausible that both the planet and the star remain bound to the SMBH. Dynamical simulations are necessary to quantify how many planets will be ejected and how many will be captured by the SMBH. If the planet is captured, its semi-major axis a_{cap} and eccentricity e_{cap} would then be (Hills 1991; Perets et al. 2009)

$$a_{\text{cap}} \simeq 1.30 \text{ pc} \left(\frac{a_p}{19 \text{ AU}} \right) \left(\frac{M_{\text{BH}}}{4 \times 10^6 M_\odot} \right)^{2/3} \left(\frac{1 M_\odot}{m_*} \right)^{2/3} \quad (3)$$

$$e_{\text{cap}} = 1 - \frac{d}{a_{\text{cap}}} \sim 0.99. \quad (4)$$

The tidal split of planets from their stars can be substantially enhanced by planet-planet scatterings, which were shown to be able to scatter Jupiter-mass planets on orbits with semi-major axis $> 50 \text{ AU}$ (Chatterjee et al. 2008; Marois et al. 2008; Chatterjee et al. 2011). The planet could even be ejected from its initial system by planet-planet scattering: Veras et al. (2009) estimate that $\sim 40\%$ of planets in a multiple-planet system are ejected by planet-planet scatterings in $2 \times 10^8 \text{ Myr}$. The ejection of Jupiter-like planets from their planet systems is supported by the observation of ‘freely floating’ giant planets (Sumi et al. 2011).

It is even possible that starless planets form directly from gravitational instabilities in accretion disks around SMBHs (Shlosman & Begelman 1989; Nayakshin 2006).

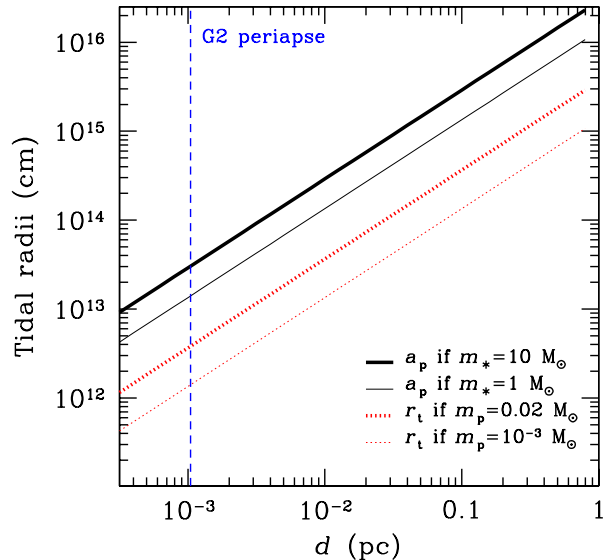


Figure 1. Tidal radius for splitting a star-planet system (solid black lines) and tidal radius for disruption of the planet (dotted red lines) as a function of the star-planet distance from the SMBH. Thick and thin solid black lines correspond to a star mass $m_* = 10$ and $1 M_\odot$, respectively. Thick and thin dotted red lines correspond to a mass $m_p = 0.02 M_\odot$ (i.e. a brown dwarf) and $10^{-3} M_\odot$ (i.e. a Jupiter-like planet), respectively. The vertical dashed line is the estimated periape distance of the G2 object.

Similarly, starless planets could have formed in the same star formation episode that gave birth to the clockwise disk: according to one of the most popular scenarios, a molecular cloud disrupted by the SMBH might have settled into a parsec-scale dense gaseous disk. Gravitational instabilities in the gaseous disk might have led to the formation of the young massive stars that lie in the clockwise disk (e.g. Paczynski 1978; Kolykhalov & Sunyaev 1980; Shlosman & Begelman 1987; Collin & Zahn 1999; Gammie 2001; Goodman 2003; Tan & Blackman 2005; Nayakshin et al. 2007; Bonnell & Rice 2008; Mapelli et al. 2008; Hobbs & Nayakshin 2009; Alig et al. 2011; Mapelli et al. 2012, 2013; Lucas et al. 2013), and also to the formation of starless giant planets (Shlosman & Begelman 1989). In such case, the initial orbit of the planets would be inside the clockwise disk, and then gravitational interactions with stars or other planets might plunge the planets on a more radial orbit. For example, Murray-Clay & Loeb (2012) predict that $\sim 1/100$ of the entire population of low-mass objects in the clockwise disk could have been delivered onto highly eccentric orbits by two-body interactions with massive stars.

What happens to a planet that is captured by the SMBH on a very eccentric orbit? Tidal disruption is unlikely, as the planet should have a radius r_p larger than

$$r_t = 1.3 \times 10^{13} \text{ cm} \frac{d}{0.01 \text{ pc}} \left(\frac{4 \times 10^6 M_\odot}{M_{\text{BH}}} \right)^{1/3} \left(\frac{m_p}{10^{-3} M_\odot} \right)^{1/3}, \quad (5)$$

i.e. $\sim 2000 (d/0.01 \text{ pc})$ times the radius of Jupiter. Fig. 1 shows the behavior of r_t as a function of d , for a planet mass $m_p = 10^{-3} M_\odot$ and for a brown dwarf of mass $m_p = 2 \times 10^{-2} M_\odot$.

2.2. Photoevaporation

The planet will suffer continuous atmosphere evaporation by the UV field of the young stars in the central parsec. According to Murray-Clay et al. (2009) (using the simplified eq. 19), the mass loss rate by atmosphere evaporation is

$$\dot{M}_{\text{MC}} \simeq \frac{\epsilon \pi r_p^2 L_{\text{UV}} / (4 \pi D^2)}{G m_p / r_p}, \quad (6)$$

where r_p is the planet radius, $L_{\text{UV}} \sim 10^{40}$ erg s⁻¹ is the ionizing luminosity of massive stars in the GC, ϵ is the fraction of the UV luminosity that goes into heat ($\simeq \tilde{\phi}/\phi_0 - 1$, where $\tilde{\phi}$ is the average energy of ionizing photons, and $\phi_0 \simeq 13.6$ eV is the ionization energy for atomic H), and D is the distance of the massive stars from the rogue planet. We assume that $D \simeq 0.1$ pc, since this is the outer rim of the clockwise disk in the GC (Yelda et al. 2014).

For large values of r_p , eq. (6) implies that the number of ionizations is larger than the number of ionizing photons reaching the planet surface,

$$Q_p = \frac{\pi r_p^2 L_{\text{UV}} / (4 \pi D^2)}{\phi_0 / (1 - \epsilon)}. \quad (7)$$

Therefore, we employ an evaporation rate

$$\begin{aligned} \dot{M} &= \min(\dot{M}_{\text{MC}}, m_{\text{prot}} Q_p) = \\ &= \frac{r_p^2 L_{\text{UV}}}{4 D^2} \frac{m_{\text{prot}}}{\phi_0} \min \left[\epsilon \frac{\phi_0 / m_{\text{prot}}}{(G m_p) / r_p}, (1 - \epsilon) \right] \simeq \\ 2.0 \times 10^{11} \text{ g s}^{-1} &\left(\frac{r_p}{10^{10} \text{ cm}} \right)^2 \left(\frac{L_{\text{UV}}}{10^{40} \text{ erg s}^{-1}} \right) \left(\frac{D}{0.1 \text{ pc}} \right)^{-2} \times \\ &\times \min \left[0.98 \epsilon \left(\frac{m_p}{10^{-3} M_\odot} \right)^{-1} \left(\frac{r_p}{10^{10} \text{ cm}} \right), (1 - \epsilon) \right], \quad (8) \end{aligned}$$

where $m_{\text{prot}} \simeq 1.67 \times 10^{-24}$ g is the proton mass. The bottom panel of Fig. 2 (dotted line) shows the behavior of \dot{M} as a function of the planet radius.

The average kinetic energy of the evaporating ions is of the order of $\sim \tilde{\phi} - \phi_0 = \epsilon [\phi_0 / (1 - \epsilon)]$, implying a velocity of the order of $v_g \sim 30$ km s⁻¹ (for $\epsilon \sim 0.3$). This velocity is generally of the same order of magnitude as the escape velocity $v_{\text{esc}} = \sqrt{(2 G m_p) / r_p}$.

Thus, the density of the ionized gas that evaporates from the star is

$$\begin{aligned} n_+ &= \frac{\dot{M}}{4 \pi m_{\text{prot}} r_p^2 v_g} = 10^7 \text{ cm}^{-3} \left(\frac{\dot{M}}{6 \times 10^{10} \text{ g s}^{-1}} \right) \\ &\left(\frac{30 \text{ km s}^{-1}}{v_g} \right) \left(\frac{10^{10} \text{ cm}}{r_p} \right)^2. \quad (9) \end{aligned}$$

The central panel of Fig. 2 (dotted line) shows n_+ (obtained assuming $v_g = v_{\text{esc}} = \sqrt{(2 G m_p) / r_p}$), as a function of the planet radius.

If the velocity of the evaporating matter is close to the escape velocity from the planet, the density profile becomes $n(r) \sim n_+(r/r_p)^{-3/2}$, and the recombination

rate can be estimated as

$$\begin{aligned} R &= \int_{r_p}^{r_{\text{max}}} 4 \pi r^2 \alpha_B n_+^2 \left(\frac{r}{r_p} \right)^{-3} dr \\ &= 4 \pi \alpha_B n_+^2 r_p^3 \ln \frac{r_{\text{max}}}{r_p} \simeq 4 \pi \alpha_B n_+^2 r_p^3 \ln \left(\frac{n_+ m_{\text{prot}}}{\rho_h} \right)^{2/3} \\ &\sim 3 \times 10^{33} \text{ s}^{-1} \left(\frac{n_+}{10^7 \text{ cm}^{-3}} \right)^2 \left(\frac{r_p}{10^{10} \text{ cm}} \right)^3 \frac{\ln \left[\frac{(n_+ m_{\text{prot}})}{\rho_h} \right]}{9.7}, \quad (10) \end{aligned}$$

where $\alpha_B \simeq 2.6 \times 10^{-13}$ cm³ s⁻¹ is the case B recombination coefficient for Hydrogen (at a temperature $\sim 10^4$ K), and we have chosen r_{max} as the radius where the density of the evaporated gas drops to the density of the hot medium: $m_{\text{prot}} n(r_{\text{max}}) \equiv \rho_h$ (the normalization of the logarithmic term is appropriate for $n_+ = 10^7$ cm⁻³, $\rho_h = 10^{-21}$ g cm⁻³). The corresponding emission measure (EM) is $\text{EM} = \int n_e^2 dV \sim 10^{45}$ cm⁻³, for $r_p = 10^{10}$ cm and $n_+ = 10^7$ cm⁻³.

Equation (10) assumes that the evaporated gas is nearly completely ionized. This is a good approximation, because the recombination time scale

$$t_{\text{rec}}(r) = \frac{1}{\alpha_B n_+(r)} \simeq 3.8 \times 10^5 \text{ s} \left(\frac{n_+}{10^7 \text{ cm}^{-3}} \right)^{-1} \left(\frac{r}{r_p} \right)^{3/2} \quad (11)$$

is longer than the ionization time scale

$$t_{\text{ion}} \sim \frac{1}{\sigma(\tilde{\phi}) L_{\text{UV}} / (4 \pi D^2 \tilde{\phi})} \simeq 1800 \text{ s} \left(\frac{10^{40} \text{ erg s}^{-1}}{L_{\text{UV}}} \right) \left(\frac{D}{0.1 \text{ pc}} \right)^2, \quad (12)$$

where we assumed that the ionization cross section of neutral Hydrogen is $\sigma(\tilde{\phi}) \simeq 6.3 \times 10^{-18}$ cm² $(\tilde{\phi}/\phi_0)^{-3} \simeq 2.1 \times 10^{-18}$ cm², which is appropriate for $\epsilon = 0.3$, i.e. $\tilde{\phi} = \phi_0 / 0.7 \simeq 19.4$ eV.

Furthermore, in this case, we can ignore the possibility of shocks with the hot medium, because the relatively low values of v_g often lead to a Mach number $\mathcal{M} = v_g / c_s \lesssim 1$, where c_s is the sound speed (slow-wind case). In the Appendix A, we discuss the case in which $\mathcal{M} \gg 1$ (fast-wind case). Photoevaporation in the fast-wind approximation leads to a recombination rate about one order of magnitude lower with respect to the slow-wind approximation, but shocks occurring in the fast-wind case enhance the recombination rate by a factor depending on \mathcal{M} (see Appendix A).

In the following, we refer to CASE 1 (see Table 1) as the model where \dot{M} , n_+ and R have been calculated from equations 8, 9 and 10, respectively (i.e. R has been calculated in the slow-wind approximation, with $v_g = \sqrt{2 G m_p / r_p}$ and $L_{\text{UV}} = 10^{40}$ erg s⁻¹). Fig. 2 (dotted line) shows \dot{M} , n_+ and R in CASE 1, as a function of the planet radius.

Table 1
Summary of model properties.

Name	\dot{M} (g s^{-1})	n_+ (cm^{-3})	R (s^{-1})	Tidal stripping
CASE 1	from eq. 8	from eq. 9	from eq. 10	no
CASE 2	from eq. 15	from eq. 14	from eq. 10	no
CASE 3	—	—	from eq. 20	yes

Note. — Columns 2, 3 and 4 specify how \dot{M} , n_+ and R were calculated in each model. CASE 1 corresponds to a photoevaporating planet (eq. 8, Section 2) in the slow-wind approximation (eq. 10), with $m_p = 10^{-3} M_\odot$, $v_g = \sqrt{2Gm_p/r_p}$ and $L_{UV} = 10^{40} \text{ erg s}^{-1}$. CASE 2 corresponds to a photoevaporating cloud (eq. 15, Section 3) in the slow-wind approximation (eq. 10) with $m_p = 10^{-3} M_\odot$, $v_g = c_s = 10 \text{ km s}^{-1}$ and $L_{UV} = 10^{40} \text{ erg s}^{-1}$. CASE 3 corresponds to a photoevaporating cloud undergoing tidal stripping ($r_p \geq r_t$), with $v_g = c_s = 10 \text{ km s}^{-1}$ and $L_{UV} = 10^{40} \text{ erg s}^{-1}$. If the cloud is being stripped, we do not need to derive \dot{M} and n_+ in order to calculate R , since $R = Q_{\text{tid}}$ (see eq. 20 and the discussion in the text).

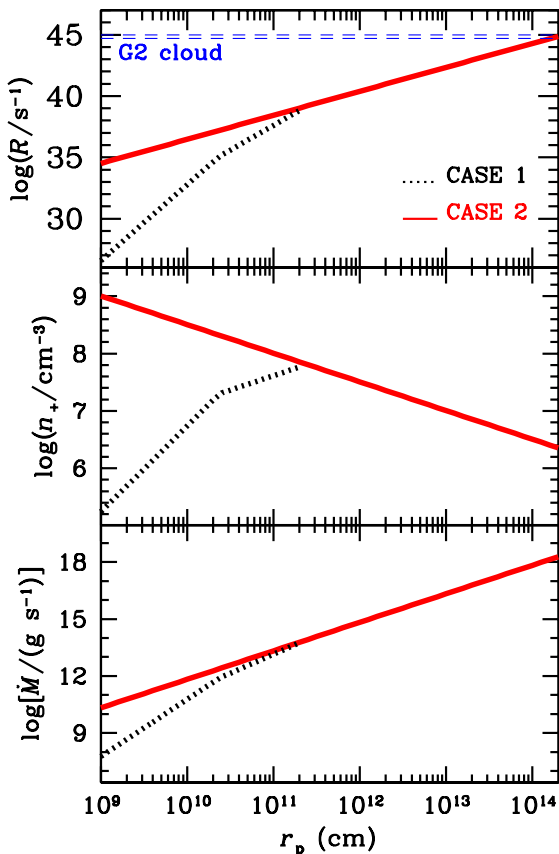


Figure 2. From top to bottom: recombination rate associated with photoevaporation (R), evaporating gas density (n_+), and mass loss rate by photoevaporation (\dot{M}) as a function of the planet (or PE) radius. Black dotted line: CASE 1 (photoevaporating planet, Table 1). CASE 1 is valid only for $r_p \leq 2 \times 10^{11} \text{ cm}$ (i.e. for $\tau < 1$, see Section 3.1 and eq. 13 for details). Red solid line: CASE 2 (photoevaporating cloud, Table 1). The two blue dashed lines in the top panel are the minimum and maximum value of the recombination rate measured for the G2 cloud in the Br γ line since 2004 (Pfuhl et al. 2014).

One of the two main competing scenarios³ for the formation of Jupiter-like planets and brown dwarfs predicts

³ In this paper, we neglect the competing core accretion model (i.e. the accretion of a gaseous atmosphere on a rocky core, e.g. Wetherill 1980; Bodenheimer & Pollack 1986; Lissauer 1993), which will be considered in forthcoming studies.

that they form through local gravitational instabilities in the outer parts of a protoplanetary disk (Kuiper 1951; Boss 1997, 1998a,b; Helled et al. 2008). The local instability might produce a protoplanetary embryo (PE): a coreless gas clump with density $\sim 10^{-8} \text{ g cm}^{-3}$ (much lower than typical planetary and stellar densities), and large radius (corresponding to a Jeans length $\lambda_J \approx$ few AU). Then, these gas clumps cool down, contracting to radii and densities typical of brown dwarfs or giant gaseous planets. Recent population synthesis studies (Forgan & Rice 2013) indicate that PEs have a mass of a few to tens of Jupiter masses, and that a large fraction of PEs ($\approx 40\text{--}90\%$) end up forming brown dwarfs (with mass $\gtrsim 0.02 M_\odot$).

One of the main predictions of this theory is that PEs can form only in the outer parts of protoplanetary disks ($\sim 10\text{--}50 \text{ AU}$ distance from the star, Forgan & Rice 2013, or even $> 100 \text{ AU}$, Boley 2009; Rafikov 2009), where the self-gravity of gas is sufficiently strong with respect to stellar gravity and radiation pressure. Thus, a PE is an excellent candidate for being tidally captured by the SMBH, before it can contract to a Jupiter-like configuration. Furthermore, starless PEs might form directly from gravitational instabilities in a dense gaseous disk surrounding the SMBH (see previous section).

3.1. Photoevaporation

For a radius of the PE $r_p < r_t \sim 1.3 \times 10^{13} \text{ cm}$ ($d/0.01 \text{ pc}$) (see eq. 5), the PE will avoid tidal disruption during the capture by the SMBH. From eq. 8, we infer that the mass loss by evaporation for a PE is $\dot{M} \sim 3.5 \times 10^{16} \text{ g s}^{-1}$ for $r_p = 5 \times 10^{12} \text{ cm}$ (and $\epsilon = 0.3$), corresponding to $n_+ \sim 2.9 \times 10^8 \text{ cm}^{-3}$ for $v_g = \sqrt{2Gm_p/r_p}$. Thus, the recombination rate for an evaporating PE would be $R \sim 3.1 \times 10^{44} \text{ s}^{-1}$ (using eq. 10), corresponding to an EM $\sim 10^{57} \text{ cm}^{-3}$. However, this result neglects the optical depth encountered by the ionizing photons before reaching the PE surface,

$$\tau = \int_{r_p}^{r_{\text{max}}} \sigma(\tilde{\phi}) n_+ \left(\frac{r}{r_p}\right)^{-3/2} \frac{t_{\text{ion}}}{t_{\text{rec}}(r)} dr \simeq 5 \times 10^{-4} \left(\frac{n_+}{10^7 \text{ cm}^{-3}}\right)^2 \left(\frac{r_p}{10^{10} \text{ cm}}\right) \left(\frac{10^{40} \text{ erg s}^{-1}}{L_{UV}}\right) \left(\frac{D}{0.1 \text{ pc}}\right)^2 \quad (13)$$

where we approximated the neutral fraction in the evaporating gas at radius r as $t_{\text{ion}}/t_{\text{rec}}(r)$ (which is correct as long as $t_{\text{ion}} \ll t_{\text{rec}}(r)$).

If we use the CASE 1 approximations at $r_p = 5 \times 10^{12} \text{ cm}$, we get $\tau \sim 200$, implying that the estimate of R is too high, since the ionizing photons would be unable to photoevaporate the surface of the PE. In general, our approximations break down when $\tau \gtrsim 1$, i.e. when $r_p \gtrsim 1 \text{ AU} (n_+/10^7 \text{ cm}^{-3})^{-2} (L_{UV}/10^{40} \text{ erg s}^{-1}) (D/0.1 \text{ pc})^{-2}$; in particular, CASE 1 holds only if $r_p \lesssim 2 \times 10^{11} \text{ cm}$.

Therefore, it is more appropriate to derive the mass loss rate \dot{M} with the assumption that the PE is a pure gas cloud (such as a protoplanetary disk). Following Murray-Clay & Loeb (2012), the mass loss rate of a gas cloud with radius r_p , which is undergoing photoevaporation, can be expressed as $\dot{M} \sim 4\pi r_p^2 m_{\text{prot}} n_+ c_s$, where

the number density of the photoevaporated ions (n_+) can be calculated assuming balance between recombinations and photoionizations at the base of the wind,

$$n_+ \approx (L_{\text{UV}} / (4\pi \tilde{\phi} D^2))^{1/2} (\alpha_B r_p)^{-1/2}, \quad (14)$$

where $\tilde{\phi}$ is the average energy of ionizing photons. Thus, the mass loss rate is

$$\begin{aligned} \dot{M} &\sim \left(\frac{4\pi}{\alpha_B}\right)^{1/2} m_{\text{prot}} c_s r_p^{3/2} \left(\frac{L_{\text{UV}}}{\tilde{\phi} D^2}\right)^{1/2} \\ &\sim 6.7 \times 10^{14} \text{ g s}^{-1} \left(\frac{c_s}{10 \text{ km s}^{-1}}\right) \left(\frac{r_p}{10^{12} \text{ cm}}\right)^{3/2} \\ &\quad \left(\frac{L_{\text{UV}}}{10^{40} \text{ erg s}^{-1}}\right)^{1/2} \left(\frac{19.4 \text{ eV}}{\tilde{\phi}}\right)^{1/2} \left(\frac{0.1 \text{ pc}}{D}\right), \end{aligned} \quad (15)$$

and the optical depth due to the evaporating gas becomes $\tau \sim 0.5$, independent of all the considered parameters, apart from $\tilde{\phi}$. This result shows that eq. (14) can be applied for a PE, since the absorption in the photoevaporative wind does not stop the photoevaporation itself.

Furthermore, if we substitute eq. (14) into eq. (10), the recombination rate becomes

$$R \simeq \frac{4\pi r_p^2 L_{\text{UV}}}{4\pi D^2 \tilde{\phi}} \ln\left(\frac{r_{\text{max}}}{r_p}\right) = \left[4 \ln\left(\frac{r_{\text{max}}}{r_p}\right)\right] Q_p, \quad (16)$$

where Q_p is the number of ionizing photons reaching the PE surface in the optically thin approximation (eq. 7). We have $R > Q_p$ because $r_{\text{max}} \gg r_p$, so that the number of available ionizing photons is much larger than Q_p .

The central and bottom panel of Fig. 2 (solid line) show the behavior of n_+ and \dot{M} , as derived from equations 14 and 15, respectively. Finally, the top panel of Fig. 2 (solid line) shows the recombination rate R obtained combining eq. 14 with eq. 10 (or, equivalently, using eq. 16). In the following, we define this model as CASE 2 (see Table 1).

3.2. Tidal stripping enhancement

The tidal radius r_t of a PE can become similar (or smaller) than its radius r_p for $d \lesssim 0.01$ pc (Fig. 1); in such case, mass loss by tidal stripping might become non-negligible at some point in the orbit. When $r_t \leq r_p$, we can estimate the mass-loss rate by tidal stripping as (Murray-Clay & Loeb 2012)

$$\begin{aligned} \dot{M}_{\text{tid}} &\sim 4\pi r_p^2 \rho(r_p) \left(\frac{m_p}{3M_{\text{BH}}}\right)^{1/3} v_{\perp} \simeq r_p^{-1} \frac{m_p^{4/3}}{(3M_{\text{BH}})^{1/3}} v_{\perp} \simeq \\ &8.7 \times 10^{22} \text{ g s}^{-1} \left(\frac{r_p}{10^{12} \text{ cm}}\right)^{-1} \left(\frac{m_p}{10^{-3} M_{\odot}}\right)^{4/3} \\ &\quad \left(\frac{v_{\perp}}{10^3 \text{ km s}^{-1}}\right) \left(\frac{M_{\text{BH}}}{4 \times 10^6 M_{\odot}}\right)^{-1/3} \end{aligned} \quad (17)$$

where we assume that the surface density of the PE is $\rho(r_p) \simeq m_p / (4\pi r_p^3)$ (appropriate in the case of an isothermal density profile), and v_{\perp} is the radial component of the orbital velocity v_p (Murray-Clay & Loeb 2012).

Which is the fate of the stripped material? How could we observe it? The tidally stripped material might undergo shocks with the high-temperature medium. The stagnation radius r_s where ram pressure is balanced

between the bow shock of the stellar wind and the hot medium is (Burkert et al. 2012; Scoville & Burkert 2013)

$$\begin{aligned} r_s &= \left(\frac{\dot{M} v_g}{4\pi \rho_h v_p^2}\right)^{1/2} = 2 \times 10^{16} \text{ cm} \left(\frac{\dot{M}_{\text{tid}}}{8.7 \times 10^{22} \text{ g s}^{-1}}\right)^{1/2} \\ &\quad \left(\frac{v_g}{10 \text{ km s}^{-1}}\right)^{1/2} \left(\frac{10^{-21} \text{ g cm}^{-3}}{\rho_h}\right)^{1/2} \left(\frac{1300 \text{ km s}^{-1}}{v_p}\right) \end{aligned} \quad (18)$$

where v_p ($\sim 1300 \text{ km s}^{-1}$) is the Kepler velocity of a planet orbiting the SMBH at 0.01 pc, and $\rho_h = 10^{-21} \text{ g cm}^{-3}$ is the density of the hot medium from X-ray measurements (Yuan et al. 2003).

Thus, the maximum luminosity that can be emitted by the tidally stripped material in such shocks is

$$\begin{aligned} L_{\text{max}} &= \pi r_s^2 \left(\frac{\rho_h}{m_{\text{prot}}}\right) \frac{1}{2} m_{\text{prot}} v_p^2 = \frac{1}{8} \dot{M}_{\text{tid}} v_g v_p \\ &\simeq 1.4 \times 10^{36} \text{ erg s}^{-1} \left(\frac{\dot{M}_{\text{tid}}}{8.7 \times 10^{22} \text{ g s}^{-1}}\right) \\ &\quad \left(\frac{v_g}{10 \text{ km s}^{-1}}\right) \left(\frac{v_p}{1300 \text{ km s}^{-1}}\right) \end{aligned} \quad (19)$$

where we used equations (18) and (17) for r_s and \dot{M}_{tid} , respectively. This luminosity is very high but can be achieved only if: (i) the stripped material reaches the stagnation radius r_s (but we estimate that the stripped gas needs $t \gtrsim 300$ yr to reach the stagnation radius, $r_s \approx 10^{16} \text{ cm}$, if it travels at $v_g \sim 10 \text{ km s}^{-1}$); (ii) all of the kinetic energy is converted into (observable) luminosity. Thus, we expect that the luminosity due to these shocks is much lower than L_{max} , and we will neglect it in the rest of this paper.

On the other hand, the stripped material will be exposed to photoevaporation by the massive young stars (Murray-Clay & Loeb 2012). The presence of the stripped material modifies the geometry of the PE and might strongly enhance photoevaporation (as discussed in Murray-Clay & Loeb 2012). To correctly evaluate the new geometry is beyond the aims of the current paper, but we can account for this correction in the following way. The surface of the stripped material will take part in photoevaporation, and will produce an approximately spherical wind.

The recombination rate in the wind will be of the same order of magnitude as the rate of ionizing photons that can be absorbed by the tidally stripped material, that is

$$Q_{\text{tid}} = \frac{4\pi r_{\text{str}}^2 L_{\text{UV}}}{4\pi D^2 \tilde{\phi}_0}, \quad (20)$$

where r_{str} is the maximum radius reached by the tidally stripped material. We evaluate r_{str} as

$$r_{\text{str}} \sim r_p + t_t v_g, \quad (21)$$

i.e. as the radius of the PE, plus the distance travelled by the stripped material (moving at velocity v_g) during the time t_t between the instant when the PE radius becomes equal to the tidal radius ($r_t = r_p$), and the time of the periape passage.

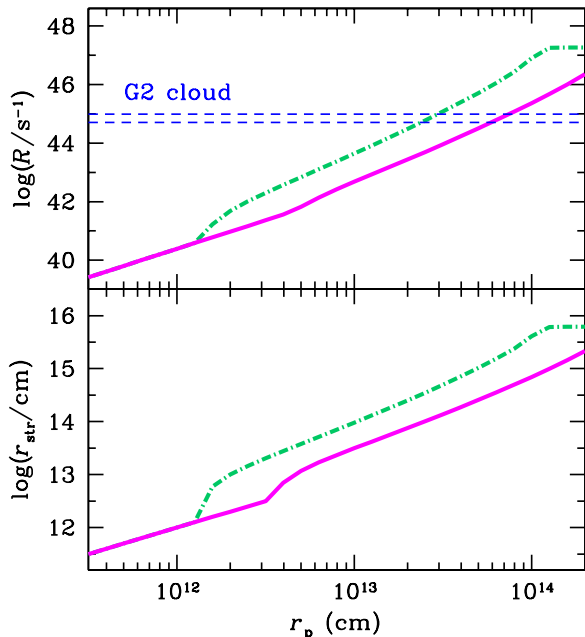


Figure 3. Bottom panel: radius r_{str} (eq. 21, assuming periape distance ~ 200 AU, eccentricity $e = 0.976$ and velocity $v_g = 10$ km s^{-1}), as a function of PE radius. A value $r_{\text{str}} = r_p$ means that r_p is smaller than r_t for the entire orbit (in this case, CASE 3 is the same as CASE 2). Top panel: recombination rate R in CASE 3 (Table 1), as a function of PE radius. R has been derived from eq. 20, assuming that $R = Q_{\text{tid}}$. In both panels, magenta solid line: PE mass $m_p = 0.02 M_\odot$; green dot-dashed line: PE mass $m_p = 10^{-3} M_\odot$. The two blue dashed lines in the top panel are the minimum and maximum value of the recombination rate measured for the G2 cloud in the Br γ line since 2004 (Pfuhl et al. 2014).

Fig. 3 shows the recombination rate⁴ R (assumed to be equal to Q_{tid}) and the radius r_{str} , as derived from equations 20 and 21, respectively. In Fig. 3, we assume $v_g = 10$ km s^{-1} , periape distance = 200 AU and eccentricity $e = 0.976$, i.e. the same periape and eccentricity as the G2 object. If $r_p > r_t$ along the entire orbit, we assume $t_t = 0.5 T_{\text{orb}}$ (where T_{orb} is the orbital period). In principle, this kind of calculation can be applied also to planets, but for the orbit of the G2 cloud r_t is always larger than r_p if $r_p \lesssim 1.5 \times 10^{12}$ cm (for $m_p = 10^{-3} M_\odot$). In the following, we refer to the model presented in Fig. 3 as CASE 3 (see Table 1).

4. DISCUSSION

4.1. Luminosity of rogue planets in the GC

Do we have any chances of detecting rogue planets or PEs in the GC with current or forthcoming facilities? The K ($2.1 \mu\text{m}$) and L' ($3.8 \mu\text{m}$) magnitudes of a rogue planet at the distance of the GC (~ 8 kpc) are $m_K \sim 32$

⁴ The calculations of Murray-Clay & Loeb (2012) are somewhat similar to ours, even if they apply to a protoplanetary disk. However, Murray-Clay & Loeb (2012) do not balance ionizations and recombinations. As illustrated by eq. (16), such balance is not required in the case of planets or PEs, because $r_{\text{max}} \gg r_p$. However, when the tidal stripping enhancement is important, the ratio $r_{\text{max}}/r_{\text{str}}$ should be of the order of unity, and $R \sim Q_{\text{tid}}$. For example, in the case of disks with radius $\gtrsim 10$ AU producing photoevaporative winds with $n \sim 10^7 \text{ cm}^{-3}$, the equations used by Murray-Clay & Loeb (2012) imply a recombination rate much larger than the ionization rate, and the material would become neutral in ~ 5 days.

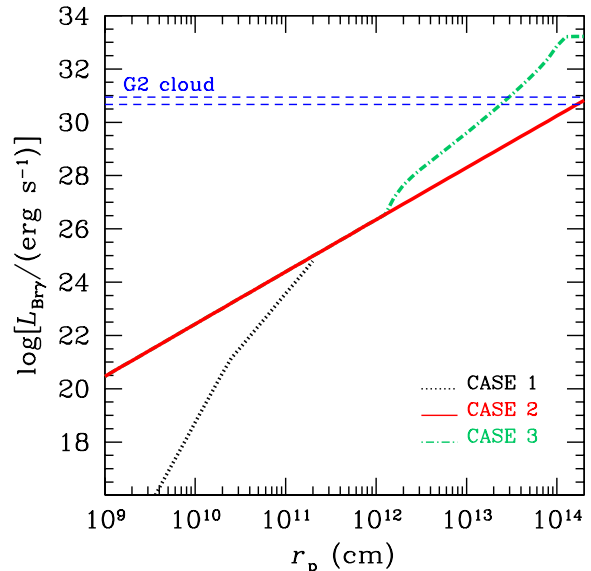


Figure 4. Br γ luminosity ($L_{\text{Br}\gamma}$) as a function of the planet (or PE) radius. The lines and colors are the same as used in Figs. 2 and 3. In particular, dotted black line: CASE 1; solid red line: CASE 2; green dash-dotted line: CASE 3 with $m_p = 10^{-3} M_\odot$. The two blue dashed lines are the minimum and maximum value of $L_{\text{Br}\gamma}$ for the G2 cloud observed since 2004 (Pfuhl et al. 2014).

and $m_{L'} \sim 26$ for a mass $m_p \sim 10^{-3} M_\odot$ (Allard et al. 2001, 2007), respectively. Therefore, such rogue planet would be invisible for current and forthcoming facilities (30-m class telescopes are expected to observe stars down to $m_K \sim 24$). On the other hand, some processes might take place that enhance the chances of observing a planet, such as tidal disruption, atmosphere evaporation and bow shocks. In the previous section, we analyzed these processes for both planets and PEs.

Fig. 4 shows the luminosity of the Br γ line ($2.166 \mu\text{m}$) derived from $L_{\text{Br}\gamma} = 2.35 \times 10^{-27} \text{ erg s}^{-1} R/\alpha_B$, where the recombination rate R was calculated in the previous section. The most optimistic prediction for a Jupiter-like planet ($m_p = 10^{-3} M_\odot$ and $r_p = 10^{10}$ cm) is a Br γ luminosity $L_{\text{Br}\gamma} \approx 5 \times 10^{18} \text{ erg s}^{-1}$, if the planet atmosphere is undergoing photoevaporation. At the distance of the GC, this corresponds to a flux $\lesssim 10^{-27} \text{ erg s}^{-1} \text{ cm}^{-2}$, which is far below the sensitivity of existing and forthcoming instruments (a 24-hr integration with VLT SINFONI can theoretically detect a Br γ flux $\sim 5 \times 10^{-18} \text{ erg s}^{-1} \text{ cm}^{-2}$ with a S/N of ~ 10).

Thus, the only chance of detecting a rogue planet in the GC is that it is disrupted and accretes onto the SMBH. If a portion of the planet mass is accreted by the SMBH, this might lead to a flare with bolometric luminosity $< 2 \times 10^{41} \text{ erg s}^{-1}$ (from eq. 45 of Zubovas et al. 2012). This event is very unlikely, because the tidal disruption occurs only if the periape distance from the SMBH is $\lesssim 1.6 \text{ AU}$ ($r_p/10^{10} \text{ cm}$). We expect a planet disruption rate $R_{\text{dis}} \sim 10^{-5} f_p \text{ yr}^{-1}$ (where f_p is the number of planets per star in the GC, and 10^{-5} yr^{-1} is the tidal disruption rate of stars estimated by Alexander 2005). This process is very rare, but might be relevant for explaining flares in other galactic nuclei.

4.2. Luminosity of rogue PEs in the GC

Theoretical models (e.g. Wuchterl 1999; Boss 2005; Helled et al. 2006; Helled & Bodenheimer 2010) suggest that a $0.001 M_{\odot}$ PE does not collapse immediately (because it is optically thick) and needs to cool for $\lesssim 1$ Myr at a bolometric luminosity $\sim 10^{-6} L_{\odot} \sim 10^{27} \text{ erg s}^{-1}$. At the distance of the GC, this luminosity corresponds to $m_{L'} \gtrsim 25$, which is far below the limits of current and forthcoming observational facilities.

The photoevaporation of the ‘atmosphere’ of a PE (with a radius of $r_p = 5 \times 10^{12}$ cm) could lead to a Br γ luminosity of $\sim 5 \times 10^{27} \text{ erg s}^{-1}$, considering CASE 2 estimates for the mass loss by photoevaporation, assuming $L_{UV} = 10^{40} \text{ erg s}^{-1}$. If the PE is undergoing tidal stripping, this luminosity might be boosted by more than 2 orders of magnitude. A $L_{Br\gamma} \approx 10^{30} \text{ erg s}^{-1}$ can be observed with current 8m telescopes, and is not far from the actual luminosity of the G2 cloud ($\sim 6 \times 10^{30} \text{ erg s}^{-1}$).

Tidal disruption of a PE occurs if the distance of the PE from the SMBH is $d \sim 750 \text{ AU}$ ($r_p/5 \times 10^{12} \text{ cm}$), suggesting that the cross section for PE disruption is a factor of $\approx 10^5$ larger than the cross section for planet disruption (neglecting gravitational focusing). This leads to a disruption rate of $\sim f_{PE} \text{ yr}^{-1}$, where f_{PE} is the number of PEs per each star.

How many PEs can form in the GC and for how long do they survive? This question contains a number of major uncertainties and we can just suggest a few hints. PEs are quite elusive objects and are expected to be relatively short-lived before they contract to Jupiter-like size ($\sim 10^{3-6} \text{ yr}$, Wuchterl 1999; Helled et al. 2008; Forgan & Rice 2013), but in the GC they could be efficiently separated from their parent star, and the strong UV flux might substantially slow down their cooling (and collapse). Furthermore, we could reverse our question, and use the non-detection of $L_{Br\gamma} \approx 10^{31} \text{ erg s}^{-1}$ objects to constrain the frequency of PEs in the GC.

4.3. Rogue PEs and the G2 cloud

The G2 cloud is the only observed object (so far) that shares similar properties with a photoevaporating and partially stripped PE. G2 probably originated from the clockwise disk in the GC, and has a very high eccentricity, $e \sim 0.976 \pm 0.007$ (Pfuhl et al. 2014). Both these constraints on the orbit are fairly consistent with the hypothesis of tidal capture of a PE (initially formed in the clockwise disk) by the SMBH, or of a dynamical ejection of the PE from the clockwise disk. It is now clear that G2 survived its periaapse passage at a distance of $\sim 200 \text{ AU}$ from the SMBH (Witzel et al. 2014), but some of its material was tidally stripped. A PE with radius $\sim 10^{12}$ cm is tidally stripped if the periaapse is $\sim 160 \text{ AU}$: such PE would not be completely tidally disrupted at a distance of $\sim 200 \text{ AU}$ from the SMBH, but it would suffer some tidal stripping.

Fig. 4 shows that the Br γ luminosity of a PE (as derived from photoevaporation and partial tidal stripping) matches the one observed for G2, if the PE has $m_p \approx 10^{-3} M_{\odot}$ and $r_p \approx 2 \times 10^{13} \text{ cm}$. If the main trigger of the Br γ emission is photoevaporation by the intense UV background in the GC, we expect the Br γ luminosity to remain roughly constant during the PE orbit. This is fairly consistent with the fact that the Br γ luminosity

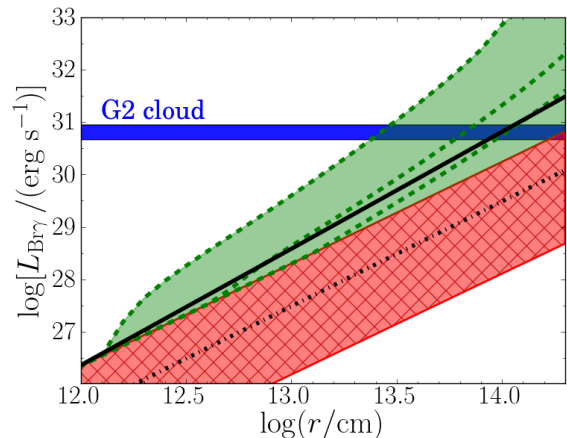


Figure 5. Uncertainties on the Br- γ luminosity of a PE. Red filled cross-hatched area: CASE 2 by varying L_{UV} from $10^{38} \text{ erg s}^{-1}$ (lower bound) to $10^{40} \text{ erg s}^{-1}$ (upper bound). Dot-dashed black line: same as CASE 2 with $L_{UV} = 10^{40} \text{ erg s}^{-1}$ but in the fast-wind approximation (with $v_g = 10 c_s$, see Appendix A, eq. A1). Solid black line: Br- γ luminosity from shocks in the fast-wind approximation (with $v_g = 10 c_s$, see Appendix A, eq. A2). Green filled area: CASE 3 with $L_{UV} = 10^{40} \text{ erg s}^{-1}$, by varying the PE mass from $10^{-3} M_{\odot}$ (upper bound) to $\sim 0.2 M_{\odot}$ (lower bound). Dashed green lines: $m_p = 10^{-3} M_{\odot}$ (top), $0.02 M_{\odot}$ (intermediate), $0.1 M_{\odot}$ (bottom). Horizontal blue filled area: the observed Br- γ luminosity of the G2 cloud (Pfuhl et al. 2014).

of G2 remained nearly constant over 10 yr (Pfuhl et al. 2014).

G2 was detected also in the L' band ($m_{L'} \sim 14$, Pfuhl et al. 2014). Gillessen et al. (2012) suggest that the continuum L' emission comes from small ($\sim 20 \text{ nm}$), transiently heated dust grains with a total warm dust mass of $\sim 2 \times 10^{23} \text{ g}$. The grains might be warmed up by an inner source (e.g. a low-mass star, Scoville & Burkert 2013; Ballone et al. 2013; Witzel et al. 2014), or by some external mechanism (UV heating, shocks, etc.). In the PE scenario, the minimum PE radius necessary to reach $L_{L'} \sim 2.1 \times 10^{33} \text{ erg s}^{-1}$ (Witzel et al. 2014) is

$$r_{\min} \sim 5.5 \times 10^{12} \text{ cm} \left(\frac{L_{L'}}{2.1 \times 10^{33} \text{ erg s}^{-1}} \right)^{1/2} \left(\frac{T_{\text{dust}}}{560 \text{ K}} \right)^{-2} \quad (22)$$

where $T_{\text{dust}} \sim 560 \text{ K}$ is the estimated dust temperature (from $L' - M' \sim 0.3$, Gillessen et al. 2012). We note that r_{\min} strongly depend on T_{dust} and that the estimate of T_{dust} is very uncertain⁵.

While the scenario of a wind-enshrouded low-mass star would naturally explain the continuum L' emission (Witzel et al. 2014), we cannot reject the hypothesis that a PE, embedded in the hot dense medium of the GC, might host sufficient warm dust to power the observed L' emission. Thus, a rogue PE might be a viable scenario to explain G2 and other G2-like objects (e.g. Pfuhl et al. 2014 suggest that the object G1 is related to G2).

4.4. Discussion of uncertainties

⁵ It should be noted that neither the radiation absorbed by the PE ($\sim 10^{31} \text{ erg s}^{-1} [L_{UV}/(10^{40} \text{ erg s}^{-1})] [D/(0.1 \text{ pc})]^{-2} [r_p/(10^{13} \text{ cm})]^2$), nor the energy released in shocks around it ($\leq 2.5 \times 10^{30} \text{ erg s}^{-1} [\rho_h/(10^{-21} \text{ g cm}^{-3})] [r_p/(10^{13} \text{ cm})]^2 [v_p/(1000 \text{ km s}^{-1})]^3$) can balance with $L_{L'}$, unless $r_p \gtrsim 5 \times 10^{13} \text{ cm}$.

The analytic model discussed in this paper relies on the possibility that planets form in the GC. The GC might be a hostile environment for planet formation, given the high UV background, the high temperature and the strong tidal field by the SMBH. Discussing the chances that planets form in the GC is beyond the aims of this paper. Here, we just mention that planetesimals and asteroids were recently investigated as possible sources of SMBH flares (Cadez et al. 2008; Kostić et al. 2009; Zubovas et al. 2012; Hamers & Portegies Zwart 2015), and there are even some observational hints for the existence of protoplanetary disks in the innermost parsec (Yusef-Zadeh et al. 2015). Further observational evidence is necessary, to confirm that planets and planetary objects form in the GC.

Planets cannot be directly observed with current and forthcoming facilities. Only photoevaporating PEs are sufficiently bright to be detected. PEs are theoretically predicted objects but have not yet been observed. They can form only if gravitational instabilities in a protoplanetary disk lead to fragmentation, and to the formation of self-gravitating clumps. Recent work has shown that gravitational instabilities can lead to the formation of PEs only in the outermost regions of a protoplanetary disk (> 100 AU, Boley 2009), where self-gravity is stronger. This enhances the probability that PEs become unbound with respect to their initial system, but might imply that their formation is endangered by the strong UV field in the GC. Furthermore, even if hydrodynamical simulations show that clumps can form, they cannot predict self-consistently whether these clumps survive further evolution.

Recent estimates suggest that PEs remain in the pre-collapse phase (the one considered in this paper) for $\sim 10^5$ yr and for $\sim 10^4$ yr if their mass is $\sim 10^{-3}$ and $10^{-2} M_\odot$, respectively (Helled et al. 2006; Helled & Bodenheimer 2010). From an observational perspective, while the detection of massive giant planets ($\gtrsim 10^{-3} M_\odot$) at distance $\gg 10$ AU from the central star might favor the gravitational instability scenario (Marois et al. 2008; see Figure 3 of Pepe et al. 2014), there is no strong evidence supporting the existence of PEs. Since PEs are such elusive objects, it is quite difficult to quantify the uncertainties in our model.

Besides the debate on the very existence of PEs, Fig. 5 shows the impact of the main sources of uncertainties on the predicted Br- γ luminosity of a photoevaporating PE. In particular, we focus on (1) the adopted approximation for the wind (fast or slow-wind approximation), (2) the flux of the UV background (from 10^{38} erg s $^{-1}$ to 10^{40} erg s $^{-1}$ in the innermost 0.1 pc), (3) the mass of the PE.

Fig. 5 shows that the Br- γ luminosity of a photoevaporating PE is uncertain by several orders of magnitude. We stress that the recombination rate (and thus the Br- γ luminosity) does not depend on the mass of the PE in CASE 2. The mass of the PE is important only if we assume that the PE can be tidally stripped by the SMBH (CASE 3), because r_t depends on the PE mass. In the fast-wind approximation (i.e. the gas is ejected with $v_g \gg v_{esc}$, as discussed in detail in Appendix A), the Br- γ luminosity due to photoevaporation (from eq. A1) is lower by about one order of magnitude with respect to the slow-wind approximation, but the gas may undergo

shocks with the hot medium, and this enhances the Br- γ luminosity to a value (from eq. A2) comparable with (or even higher than) the slow-wind approximation.

5. SUMMARY

In this paper, we investigated the possible observational signatures of planets and planetary embryos (PEs) in the GC. If planets and PEs form in the central parsec, several mechanisms can separate them from their parent star (e.g. tidal shear by the SMBH or planet-planet scatterings), and bring them onto a very eccentric orbit around the SMBH. It is even possible that starless PEs and planets form directly from gravitational instabilities in a dense gas disk around the SMBH (such as the one that might have given birth to the clockwise disk of young massive stars).

We have shown that both planets and PEs suffer from photoevaporation (Fig. 2) due to the intense UV background. The emission measure associated with such process is relatively low for planets ($EM \sim 10^{45}$ cm $^{-3}$) and much higher, although very uncertain, for PEs ($EM \sim 10^{50-56}$ cm $^{-3}$). In the case of PEs, tidal stripping can enhance the effect of photoevaporation, leading to an even higher EM (up to $EM \approx 10^{60}$ cm $^{-3}$, Fig. 3). This means that a photoevaporating PE with radius $\sim 5 \times 10^{13}$ cm might reach a Br- γ luminosity $L_{Br\gamma} \approx 5 \times 10^{29}$ erg s $^{-1}$ if it is not tidally stripped, and $L_{Br\gamma} \approx 5 \times 10^{31}$ erg s $^{-1}$ if it is partially tidally stripped (Fig. 4). This value, while uncertain, is remarkably similar to the observed Br- γ luminosity of the G2 dusty object. Furthermore, a PE with radius $\gtrsim 5 \times 10^{13}$ cm can emit the same $L_{L'}$ luminosity as G2, if it contains the sufficient amount of dust at temperature ≈ 600 K. In our model, the L' luminosity is emitted from a smaller area than the Br- γ line, since the former is due to dust inside the PE, while the latter is produced by the photoevaporative wind. This can account for the fact that the observed L' emission is more compact than the emission in Br- γ (Witzel et al. 2014). If G2 is a PE with radius $\sim 5 \times 10^{13}$ cm, we expect its lifetime to be $t_{life} \approx 10^5$ yr ($m_p/10^{-3}M_\odot$) (5×10^{17} g s $^{-1}/\dot{M}$), but tidal stripping can reduce t_{life} significantly (down to ≈ 100 yr).

Our results are affected by several uncertainties. First, PEs are theoretically predicted objects, but elusive to observe. Their properties and survival time are uncertain. Furthermore, the luminosity of photoevaporating PEs strongly depends on several quantities (e.g. PE mass, UV background luminosity, wind speed), as shown in Fig. 5. In a follow-up work we will investigate the hydrodynamical evolution of PE models embedded in a UV background. Furthermore, the frequency of PEs in the GC, and the probability that they are captured by the SMBH deserves further study. Our preliminary results open a new exciting window on GC's environment.

ACKNOWLEDGMENTS

We thank Mariangela Bonavita and Alessia Gualandris for useful discussions. MM acknowledges financial support from the Italian Ministry of Education, University and Research (MIUR) through grant FIRB 2012 RBF12PM1F, and from INAF through grants PRIN-2011-1 and PRIN-2014-14. ER acknowledges financial support from Progetto di Ateneo 2012, University of

Padova, ID: CPDA125588/12.

APPENDIX

A. THE FAST-WIND APPROXIMATION

In the main text, we discussed the case in which $v_g \lesssim v_{\text{esc}}$. While this is the more likely scenario, in this appendix we also consider the case in which the initial velocity $v_g \gg v_{\text{esc}}$. If $v_g \gg v_{\text{esc}}$, we can assume that v_g remains approximately constant, so that the gas density scales as $n(r) \sim n_+(r/r_p)^{-2}$. Thus, we can estimate the recombination rate as as

$$\begin{aligned} R &= \int_{r_p}^r 4\pi r_{\text{max}}^2 \alpha_B n_+^2 \left(\frac{r}{r_p}\right)^{-4} dr \\ &= 4\pi \alpha_B n_+^2 r_p^3 \left(1 - \frac{r_p}{r_{\text{max}}}\right) \\ &\sim 3.3 \times 10^{32} \text{s}^{-1} \left(\frac{n_+}{10^7 \text{cm}^{-3}}\right)^2 \left(\frac{r_p}{10^{10} \text{cm}}\right)^3, \quad (\text{A1}) \end{aligned}$$

where $\alpha_B \sim 2.6 \times 10^{-13} \text{cm}^3 \text{s}^{-1}$ is the Case B radiative recombination coefficient for H (at a temperature of $\sim 10^4$ K), and r_{max} (typically $\gg r_p$) is the outer limit of the wind-dominated density profile (either the radius where the interaction between the wind and the high-temperature medium produces a shock - see below -, or the radius where the wind density drops below that of the surrounding medium). A recombination rate $R \sim 1.2 \times 10^{33} \text{s}^{-1}$ corresponds to an emission measure $\text{EM} = \int n_e^2 dV \sim 3 \times 10^{46} \text{cm}^{-3}$.

The wind that evaporates from the planet will also undergo a shock with the high-temperature medium in the GC. Equation 18 in Section 3.2 provides the stagnation radius r_s where ram pressure is balanced between the bow shock of the stellar wind and the hot medium (Burkert et al. 2012; Scoville & Burkert 2013).

We estimate the combined effect of the shock and the photoevaporation with a simplified version of the results of Dyson (1975): we assume that the results along the direction of motion are approximately valid for all directions, obtaining a recombination rate

$$\begin{aligned} \tilde{R} &\simeq 4\pi \alpha_B n_+^2 r_p^3 \left(1 + \frac{r_p}{r_s} \mathcal{M}^2\right) \\ &\sim 2.5 \times 10^{33} \text{s}^{-1} \left(\frac{n_+}{10^7 \text{cm}^{-3}}\right)^2 \left(\frac{r_p}{10^{10} \text{cm}}\right)^3. \quad (\text{A2}) \end{aligned}$$

Equation A2 holds only if $\mathcal{M}^2 \gg 1$, where $\mathcal{M} \equiv v_g/c_s$ is the Mach number, and c_s is the sound speed (the normalization used in eq. A2 adopts $\mathcal{M} = 5$, corresponding to $v_g = 50 \text{km s}^{-1}$, and $c_s = 10 \text{km s}^{-1}$). Thus, the contribution of shocks increases the recombination rate by a factor of ≈ 8 for $\mathcal{M} = 5$. In Fig. 5, we compare the Br- γ luminosity of a PE in the slow-wind approximation and in the fast-wind approximation.

REFERENCES

- Alexander, T. 2005, *PhR*, 419, 65
 Alig, C., Burkert, A., Johansson, P. H., Schartmann, M. 2011, *MNRAS*, 412, 469
 Allard, F., Hauschildt, P. H., Alexander, D. R., Tamanai, A., Schweitzer, A. 2001, *ApJ*, 556, 357
 Allard, F., Allard, N. F., Homeier, D., Kielkopf, J., McCaughrean, M. J., Spiegelman, F. 2007, *A&A*, 474, L21
 Ballone, A., Schartmann, M., Burkert, A., Gillessen, S., Genzel, R., Fritz, T. K., Eisenhauer, F., Pfuhl, O., Ott, T. 2013, *ApJ*, 776, 13
 Bartko, H., Martins, F., Fritz, T. K., Genzel, R., Levin, Y., Perets, H.B., Paumard, T., Nayakshin, S., Gerhard, O., Alexander, T., et al. 2009, *ApJ*, 697, 1741
 Bodenheimer, P., Pollack, J. B. 1986, *Icarus*, 67, 391
 Boley, A. C. 2009, *ApJ*, 695, L53
 Bonnell, I. A., Rice, W. K. M. 2008, *Science*, 321, 1060
 Boss, A. P. 1997, *Science*, 276, 1836
 Boss, A. P. 1998a, *ApJ*, 503, 923
 Boss, A. P. 1998b, *Nature*, 395, 320
 Boss, A. P. 2005, *ApJ*, 629, 535
 Burkert, A., Schartmann, M., Alig, C., Gillessen, S., Genzel, R., Fritz, T. K., Eisenhauer, F. 2012, *ApJ*, 750, 58
 Cadez, A., Calvani, M., Kostić, U. 2008, *A&A*, 487, 527
 Cameron, A. G. W. 1978, *Moon and the Planets*, 18, 5
 Chatterjee, S., Ford, E. B., Matsumura, S., Rasio, F. A. 2008, *ApJ*, 686, 580
 Chatterjee, S., Ford, E. B., Rasio, F. A. 2011, in *The Astrophysics of Planetary Systems: Formation, Structure, and Dynamical Evolution*, Proceedings of the International Astronomical Union, IAU Symposium, 276, 225
 Collin, S., Zahn, J.-P. 1999, *A&A*, 344, 433
 De Colle, F., Raga, A. C., Contreras-Torres, F. F., Toledo-Roy, J. C. 2014, *ApJ*, 789, L33
 Durisen, R. H., Boss, A. P., Mayer, L., Nelson, A. F., Quinn, T., Rice, W. K. M. 2007, *Protostars and Planets V*, B. Reipurth, D. Jewitt, and K. Keil (eds.), University of Arizona Press, Tucson, p. 607
 Dyson, J. E. 1975, *Ap&SS*, 35, 299
 Forgan, D., Rice, K. 2013, *MNRAS*, 432, 3168
 Gammie, Ch. F. 2001, *ApJ*, 553, 174
 Genzel, R., Schödel, R., Ott, T., Eisenhauer, F., Hofmann, R., Lehnert, M., Eckart, A., Alexander, T., Sternberg, A., Lenzen, R., et al. 2003, *ApJ*, 594, 812
 Gillessen, S., Eisenhauer, F., Fritz, T. K., Bartko, H., Dodds-Eden, K., Pfuhl, O., Ott, T., Genzel, R. 2009a, *ApJ*, 707, L114
 Gillessen, S., Eisenhauer, F., Trippe, S., Alexander, T., Genzel, R., Martins, F., Ott, T. 2009b, *ApJ*, 692, 1075
 Gillessen, S., Genzel, R., Fritz, T. K., Quataert, E., Alig, C., Burkert, A., Cuadra, J., Eisenhauer, F., Pfuhl, O., Dodds-Eden, K., Gammie, C. F., Ott, T. 2012, *Nature*, 481, 51
 Gillessen, S., Genzel, R., Fritz, T. K., Eisenhauer, F., Pfuhl, O., Ott, T., Cuadra, J., Schartmann, M., Burkert, A. 2013, *ApJ*, 763, 78
 Ginsburg, I., Loeb, A., Wegner, G. A. 2012, *MNRAS*, 423, 948
 Goodman, J. 2003, *MNRAS*, 339, 937
 Guillochon, J., Loeb, A., MacLeod, M., Ramirez-Ruiz, E. 2014, *ApJ*, 786, L12
 Hamers, A. S., Portegies Zwart, S. F. 2015, *MNRAS*, 446, 710
 Helled, R., Podolak, M., Kovetz, A. 2006, *Icarus*, 185, 64
 Helled, R., Podolak, M., Kovetz, A. 2008, *Icarus*, 195, 863
 Helled, R., Bodenheimer, P. 2010, *Icarus*, 207, 503
 Hills, J. G. 1991, *AJ*, 102, 704
 Hobbs, A., Nayakshin, S. 2009, *MNRAS*, 394, 19
 Jackson, J. M., Geis, N., Genzel, R., Harris, A. I., Madden, S., Poglitsch, A., Stacey, G. J., Townes, C. H. 1993, *ApJ*, 402, 173
 Kolykhalov, P. I., Syunyaev, R. A. 1980, *Soviet Astronomy Letters*, 6, 357
 Kostić, U., Cadez, A., Calvani, M., Gomboc, A. 2009, *A&A*, 496, 307
 Kuiper, G. P. 1951, *Proceedings of the National Academy of Sciences of the United States of America*, 37, 1
 Lissauer, J. J. 1993, *ARA&A*, 31, 129
 Liu, H. B., Hsieh, P.-Y., Ho, P. T. P., Su, Y.-N., Wright, M., Sun, A.-L., Minh, Y. C. 2012, *ApJ*, 756, 195
 Lu, J. R., Ghez, A. M., Hornstein, S. D., Morris, M. R., Becklin, E. E., Matthews, K. 2009, *ApJ*, 690, 1463
 Lu, J. R., Do, T., Ghez, A. M., Morris, M. R., Yelda, S., Matthews, K. 2013, *ApJ*, 764, 155
 Lucas, W. E., Bonnell, I. A., Davies, M. B., Rice, W. K. M. 2013, *MNRAS*, 433, 353

- Mapelli, M., Hayfield, T., Mayer, L., Wadsley, J. 2008, arXiv0805.0185
- Mapelli, M., Hayfield, T., Mayer, L., Wadsley, J. 2012, *ApJ*, 749, 168
- Mapelli, M., Gualandris, A., Hayfield, T. 2013, *MNRAS*, 436, 3809
- Mapelli, M., Gualandris, A., Star Formation and Dynamics in the Galactic Centre, invited review paper, 2015, to appear as a chapter of the book 'Astrophysical Black Holes', in the Lecture Notes in Physics, published by Springer
- Marois, C., Macintosh, B., Barman, T., Zuckerman, B., Song, I., Patience, J., Lafrenière, D., Doyon, R. 2008, *Science* 322, 1348
- McCourt, M., O'Leary, R. M., Madigan, A.-M., Quataert, E. 2015, *MNRAS*, submitted, 2014arXiv1409.6719
- Meyer, F., Meyer-Hofmeister, E. 2012, *A&A*, 546, L2
- Miralda-Escudé, J. 2012, *ApJ*, 756, 86
- Murray-Clay, R. A., Chiang, E. I., Murray, N. 2009, *ApJ*, 693, 23
- Murray-Clay, R. A., Loeb, A. 2012, *Nature Communications*, 3, 1049
- Nayakshin, S. 2006, *MNRAS*, 372, 143
- Nayakshin, S., Cuadra, J., Springel, V. 2007, *MNRAS*, 379, 21
- Nayakshin, S., Sazonov, S., Sunyaev, R. 2012, *MNRAS*, 419, 1238
- Paczynski, B. 1978, *Acta Astronomica* 28, 91
- Paumard, T., Genzel, R., Martins, F., Nayakshin, S., Beloborodov, A. M., Levin, Y., Trippe, S., Eisenhauer, F., Ott, T., Gillessen, S., et al. 2006, *ApJ*, 643, 1011
- Pepe, F., Ehrenreich, D., Meyer, M. R. 2014, *Nature*, 513, 358
- Perets, H. B., Gualandris, A., Kupa, G., Merritt, D., Alexander, T. 2009, *ApJ*, 702, 884
- Pfahl, E. 2005, *ApJ*, 626, 849
- Pfuhl, O., Gillessen, S., Eisenhauer, F., Genzel, R., Plewa, P. M., Ott, T., Ballone, A., Schartmann, M., Burkert, A., Fritz, T. K. 2015, *ApJ*, 798, 111
- Ponti, G., Terrier, R., Goldwurm, A., Belanger, G., Trap, G. 2010, *ApJ*, 714, 732
- Prodan, S., Antonini, F., Perets, H. B. 2015, *ApJ*, 799, 118
- Rafikov, R. R. 2009, *ApJ*, 704, 281
- Revnivtsev, M. G., Churazov, E. M., Sazonov, S. Yu., Sunyaev, R. A., Lutovinov, A. A., Gilfanov, M. R., Vikhlinin, A. A., Shtykovsky, P. E., Pavlinsky, M. N. 2004, *A&A*, 425, L49
- Schödel, R., Eckart, A., Alexander, T., Merritt, D., Genzel, R., Sternberg, A., Meyer, L., Kul, F., Moulata, J., Ott, T., Straubmeier, C. 2007, *A&A*, 469, 125
- Schartmann, M., Burkert, A., Alig, C., Gillessen, S., Genzel, R., Eisenhauer, F., Fritz, T. K. 2012, *ApJ*, 755, 155
- Scoville, N., Burkert, A. 2013, *ApJ*, 768, 108
- Scoville, N. Z., Stolovy, S. R., Rieke, M., Christopher, M., Yusef-Zadeh, F. 2003, *ApJ*, 594, 294
- Shcherbakov, R. V. 2014, *ApJ*, 783, 31
- Shlosman, I., Begelman, M. C. 1987, *Nature*, 329, 810
- Shlosman, I., Begelman, M. C. 1989, *ApJ*, 341, 685
- Sumi, T., Kamiya, K., Bennett, D. P., Bond, I. A., Abe, F., Botzler, C. S., Fukui, A., Furusawa, K., Hearnshaw, J. B., Itow, Y. 2011, *Nature*, 473, 349
- Tan, J. C., Blackman, E. G. 2005, *MNRAS*, 362, 983
- Terrier, R., Ponti, G., Bélanger, G., Decourchelle, A., Tatischeff, V., Goldwurm, A., Trap, G., Morris, M. R., Warwick, R. 2010, *ApJ*, 719, 143
- Veras, D., Crepp, J. R., Ford, E. B. 2009, *ApJ*, 696, 1600
- Wetherill, G. W. 1980, *ARA&A*, 18, 77
- Witzel, G., Ghez, A. M., Morris, M. R., Sitarski, B. N., Boehle, A., Naoz, S., Campbell, R., Becklin, E. E., Canalizo, G., Chappell, S., et al. 2014, *ApJ*, 796, L8
- Wuchterl, G. 1999, *Bulletin of the Astronomical Society*, 31, 1130
- Yelda, S., Ghez, A. M., Lu, J. R., Do, T., Meyer, L., Morris, M. R., Matthews, K. 2014, *ApJ*, 783, 131
- Yuan, F., Quataert, E., Narayan, R. 2003, *ApJ*, 598, 301
- Yusef-Zadeh, F., Roberts, D. A., Wardle, M., Cotton, W., Schödel, R., Royster M. J. 2015, *ApJL*, in press, arXiv:1502.03109
- Zubovas, K., Nayakshin, S., Markoff, S. 2012, *MNRAS*, 421, 1315